ELSEVIER

Probabilistic Engineering Mechanics 15 (2000) 139–153

PROBABILISTIC ENGINEERING MECHANICS

www.elsevier.com/locate/probengmech

# Application of load-dependent Ritz vectors to Bayesian probabilistic damage detection

Hoon Sohn, Kincho H. Law*

*Department of Civil and Environmental Engineering, Stanford University, Stanford, CA 94305-4020, USA*

Received 21 September 1997; received in revised form 4 September 1998; accepted 16 September 1998

**Abstract**

This paper demonstrates the possibility of incorporating load-dependent Ritz vectors as an alternative to modal parameters into a Bayesian probabilistic framework for detecting damages in a structure. Recent research has shown that it is possible to extract load-dependent Ritz vectors from vibration tests. This paper shows that load-dependent Ritz vectors have the following potential advantages for damage detection over modal vectors: (1) in general, load-dependent Ritz vectors are more sensitive to damage than the corresponding modal vectors; and (2) substructures of interest can be made more observable using the load-dependent Ritz vectors generated from particular load patterns. An eight-bay truss example and a five-story frame example, explicitly considering both modeling error and measurement noise, are presented to illustrate the applicability of the proposed approach. 

*Keywords*: Bayesian probabilistic approach; Damage detection; Load-dependent Ritz vector; Sensitivity analysis; Modeling error

## 1. Introduction

Damage detection and health monitoring of large-scale structures are important challenges to engineering research. One common approach is to employ the vibration characteristics of a structure to predict the damage locations and to estimate the amount of damage [3]. It was shown that changes in the modal parameters might not be apparent at an early stage of damage [6,12]. Also, the uncertainties caused by measurement noise, modeling error involved in an analytical model, and environmental changes such as variations in temperature and load conditions can impede reliable identification of damage [7]. Therefore, for reliable damage detection, damage would need to cause significant changes in the modal parameters that are beyond the natural variability caused by the effects other than damage.

To overcome the insensitivity of modal vectors, several alternatives were proposed. Pandey et al. [15] compute the mode shape curvature from the displacement mode shape, and demonstrate that the changes in the mode shape curvature can be a good indicator of damage for beam structures. Stubbs et al. [18] present a damage index method which measures the decrease of modal strain energy before and after damage occurrence. These two techniques were applied successfully to the damage detection of the I-40 bridge in Albuquerque, New Mexico [8]. Yao et al. [19] apply the strain mode shape to identify local damage of a braced steel frame structure. The idea is that the force redistribution caused by damage can be related to the change of the strain mode shape. These methods require the direct measurement of dynamic strains or the derivatives of the measured displacement mode shapes to compute the strain mode shape or mode shape curvature. However, the noise induced by the measurement of dynamic strains is generally higher than that by typical accelerometer measurement. Furthermore, numerical procedures to compute the curvature from the displacement also inevitably produce errors. Cao and Zimmerman [2] show that it is possible to experimentally extract Ritz vectors from the traditional modal analysis using accelerometers. Ritz vectors (or Lanczos vectors) were shown very effective for dynamic and earthquake analyses, eigenvalue problems and model reductions. However, very few studies have applied Ritz vectors to damage detection or system identification problems [1, 13]. It should be noted that since, similar to modal vectors, Ritz vectors simply serve as a basis to expand the displacement space, they can be easily employed in the aforementioned strain mode shape/mode shape curvature based techniques.

In this paper, the possibility of incorporating load-dependent Ritz vectors into the previously proposed Bayesian probabilistic framework is investigated [17]. The idea is to

* Corresponding author.
*E-mail address:* law@ce.stanford.edu (K.H. Law).

0266-8920/00/$ - see front matter 
PII: S0266-8920(98)00044-7

search for the most probable damage event by comparing the relative probabilities for different damage scenarios, where the relative probability of a damage event is expressed in terms of the posterior probability of the damage event, given the estimated data sets from the structure. The approach described in this paper is analogous to the pattern recognition using a Bayes classifier [9]. The goal of the pattern recognition approach is to make a decision, when a new measurement is observed, whether the measurement comes from normal (healthy) or abnormal (damaged) states of a system. To make this decision, the Bayes classifier assumes a probabilistic distribution of each class, and to estimate the characteristic parameters of each distribution from observations. However, the difficulty of obtaining the sample observations hampers the application of the Bayes classifier to damage detection problems, the collection of sample observations corresponding to the damaged state of the specific location is practically infeasible unless the structure is intentionally damaged. To overcome this difficulty, Garcia and Stubbs [10] estimate the properties of the undamaged and damaged classes from a finite element (FE) model of the structure with simulated damages. The performance of this approach depends on the selection of the simulated data sets used to estimate the class properties. Theoretically, for a structure with $n$ number of substructures, $2^{n-1}$ different damage scenarios need to be simulated to correctly estimate the properties of a single class. This process needs to be repeated for the damaged/undamaged classes for all the substructures. Furthermore, if a different damage amount for each substructure is considered, the computation becomes practically prohibitive.

The proposed approach eliminates the parameter estimation process by defining each damage scenario as a separate class. In addition, a branch-and-bound search scheme is proposed to reduce the computations and to expedite the search for the most likely damage event without exhaustively examining all the possible classes [17]. This paper is motivated by the following potential advantages of Ritz vectors over the modal vectors: (1) in general, Ritz vectors are more sensitive to damage than the corresponding modal vectors; (2) substructures of interest can be made more observable using the Ritz vectors generated from particular load patterns; (3) the computation of Ritz vectors is less expensive than that of modal vectors (eigenvectors); and (4) while the practical difficulties of modal testing impede the extraction of a large number of meaningful modes, a larger number of Ritz vectors can be extracted by imposing different load patterns on a structure.

Sensitivity analyses of modal vectors [12,16] reveal that only members (or substructures) which cause significant changes in the estimated modal parameters can be detected and the sensitivity of each mode varies according to damage locations. Therefore, a weighting or selection scheme of modal vectors is desirable to measure the relative significance of the modal vectors to damage [4]. However, since the actual damage locations are not known a priori, the mode selection scheme becomes difficult. In this study, we measure the relative significance of Ritz vectors to the assumed damage locations for the computation of the posterior probability. That is, components of Ritz vectors, which are sensitive to the assumed damage locations, are weighted for the posterior probability computation of each damage case.

This paper is organized as follows: The next section describes the theoretical formulation of the previously proposed Bayesian probabilistic approach, the weighting scheme and the derivation of Ritz vector sensitivities. Section 3 presents numerical examples to illustrate the effectiveness of the proposed method. Section 4 summarizes this paper and discusses future work.

## 2. Theoretical formulation

This section first reviews the Bayesian framework for damage detection [17]. Second, a weighting scheme is introduced into the Bayesian framework to consider measurement uncertainties and sensitivities of Ritz vectors to damage. Third, the sensitivity of Ritz vectors is derived along with the generation procedure of the Ritz vectors.

### 2.1. Formulation of Bayesian framework

For an analytical model with $N_{\text{sub}}$ substructures, the system stiffness matrix $\mathbf{K}$ can be expressed as an assembly of substructure stiffness matrices $\mathbf{K}_{si}$:

$$\mathbf{K}(\Theta) = \sum_{i-1}^{N_{\text{sub}}} \theta_i \mathbf{K}_{si} \tag{1}$$

where $\Theta = \{\theta_i; i = 1, \ldots, N_{\text{sub}}\}$ and $\theta_i (0 \le \theta_i \le 1)$ is a nondimensional parameter which represents the contribution of the $i$th substructure stiffness to the system stiffness matrix. A substructure is defined as damaged when the $\theta$ value is less than a specified threshold.

When vibration tests are repeated $N_s$, times, the total collection of $N_s$, data sets is denoted as:

$$\hat{\Psi}_{N_s} = \{\hat{\psi}(n) : n = 1, \ldots, N_s\} \tag{2}$$

Each data set $\hat{\psi}(n)$ is composed of Ritz vectors estimated from the $n$th vibration test:

$$\hat{\psi}(n) = [\hat{\boldsymbol{r}}_1^{n\mathrm{T}}, \ldots, \hat{\boldsymbol{r}}_{N_r}^{nT}]^{\mathrm{T}} \in \mathbf{R}^{N_t} \tag{3}$$

where $\hat{\boldsymbol{r}}_i^n$ denotes the $i$th estimated Ritz vector in the $n$th data set $\hat{\psi}(n)$. The Ritz vector $\hat{\boldsymbol{r}}_i^n$ ($\hat{\boldsymbol{r}}_i \in \mathbf{R}^{N_d}$) has components corresponding to the instrumented DOFs. The variables $N_t$, $N_d$ and $N_r$, represent the total number of components in a data set $\hat{\psi}(n)$, the number of the measured DOFs and the number of the estimated Ritz vectors, respectively.

Let $H_j$ denote a hypothesis for a damage event which can contain any number of substructures as damaged, and the initial degree of belief about the hypothesis $H_j$ is represented by a prior probability $P(\mathrm{H_j})$. Using Bayes Theorem, the

posterior probability $P(H_j|\hat{\Psi}_{N_s})$, after observing the estimated data sets $\hat{\Psi}_{N_s}$, is given as:

$$P(H_j|\hat{\Psi}_{N_s}) = \frac{P(\hat{\Psi}_{N_s}|H_j)}{P(\hat{\Psi}_{N_s})}P(H_j) \tag{4}$$

The most likely damaged substructures are the ones included in the hypothesis $H_{\max}$ which has the largest posterior probability, i.e.

$$P(H_{\max}|\hat{\Psi}_{N_s}) = \max_{\forall H_j} P(H_j|\hat{\Psi}_{N_s}) \tag{5}$$

Since the objective is to determine the most probable damage hypothesis (event), only the relative posterior probabilities of alternative hypotheses are of interest. We attempt to avoid the explicit expression of a posterior probability $P(H_j|\hat{\Psi}_{N_s})$ since the precise calculation of $P(\hat{\Psi}_{N_s}|H_j)$ is a difficult task. To overcome these difficulties, we focus on the relative comparisons of posterior probabilities. We have shown that the comparison of posterior probabilities can be conducted by examining the error function $J(\hat{\Psi}_{N_s}, \Theta_{H_j})$ and the prior probability $P(\mathrm{H_j})$ [17]:

$$J(\hat{\Psi}_{N_s}, \Theta_{H_{\max}}^{\max}) - lnP(H_{\max}) = \min_{\forall H_j}[J(\hat{\Psi}_{N_s}, \Theta_{H_j}^{\max}) - lnP(H_j)] \tag{6}$$

$J(\hat{\Psi}_{N_s}, \Theta_{H_j})$ is defined as:

$$J(\hat{\Psi}_{N_s}, \Theta_{H_j}) = \frac{1}{2}\sum_{n=1}^{N_s}[\hat{\psi}(n) - \psi(\Theta_{H_j}) - e_{\mathrm{M}}(\Theta_{H_j})]^{\mathrm{T}}\mathbf{C}_{\hat{\Psi}}^{-1}[\hat{\psi}(n) - \psi(\Theta_{H_j}) - e_{\mathrm{M}}(\Theta_{H_j})] \tag{7}$$

where $\mathbf{C}_{\hat{\Psi}}$ is the covariance matrix of $\hat{\psi}$ and an analytical data set $\psi(\Theta_{H_j})$ given $\Theta_{H_j}$, is defined similar to Eq. (3):

$$\psi(\Theta_{H_j}) = [\boldsymbol{r}_1^{\mathrm{T}}(\Theta_{H_j}), \ldots, \boldsymbol{r}_{N_r}^{\mathrm{T}}(\Theta_{H_j})]^{\mathrm{T}} \in \mathbf{R}^{N_t} \tag{8}$$

The term $e_{\mathrm{M}}(\Theta_{H_j})$ in Eq. (7) is the output error caused by the discrepancy between the measured response of the structure and the response of the associated analytical model. When damage is not severe, the modeling error is assumed not to change significantly and the output error caused by the modeling error, $e_{\mathrm{M}}(\Theta_{H_j})$, can be approximated by $e_{\mathrm{M}}(\Theta_{H_o})$. Here, $e_{\mathrm{M}}(\Theta_{H_o})$ can be evaluated from the mean Ritz vector set $\hat{\psi}_m^h$ of the healthy structure and the Ritz vector set $\psi(\Theta_{H_o})$ of the initial analytical model:

$$e_{\mathrm{M}}(\Theta_{H_j}) \cong e_{\mathrm{M}}(\Theta_{H_o}) = \hat{\psi}_m^h - \psi(\Theta_{H_o}); \forall \Theta_{H_j} \tag{9}$$

where the $i$th component of $\hat{\psi}_{m,i}^h$ is computed using $N_{\mathrm{s}}^h$ number of Ritz vector sets, $\hat{\psi}^h(n)$ $(n = 1, \ldots, N_{\mathrm{s}}^h)$, obtained from the healthy structure:

$$\hat{\psi}_{m,i}^h = \frac{1}{N_{\mathrm{s}}^h}\sum_{n=1}^{N_{\mathrm{s}}^h}\hat{\psi}_i^h(n) \qquad \text{for } i = 1, \ldots, N_{\mathrm{t}} \tag{10}$$

The most probable parameter values $\Theta_{H_j}^{\max}$, given a hypothesis $H_j$, is sought such that:

$$f(\Theta_{H_j}^{\max}|\hat{\Psi}_{N_s}) = \max_{\Theta_{H_j} < \Omega_{H_j}^*} f(\Theta_{H_j}|\hat{\Psi}_{N_s}) \tag{11}$$

If we define $\Theta_{H_j}^1$ as a set of $\theta_j$'s corresponding to the damaged substructures in a hypothesis $H_j$ and $\Theta_{H_j}^2$ as the remaining $\theta_j$'s, the search space for $\Theta_{H_j}^{\max}$ becomes such that $0 \le \Theta_{H_j}^1 \le \Theta_{H_j}^{1,*}$ and $\Theta_{H_j}^{2,*} < \Theta_{H_j}^2 \le 1$. Here, $\Theta_{H_j}^{1,*}$ and $\Theta_{H_j}^{2,*}$ are the sets of damage thresholds for $\Theta_{H_j}^1$ and $\Theta_{H_j}^2$, respectively. $\Theta_{H_j}\Omega_{H_j}^*$ in Eq. (11) denotes this search space. Furthermore, the conditional joint PDF in Eq. (11) is defined as:

$$f(\Theta_{H_j}|\hat{\Psi}_{N_s}) = \frac{1}{[2\pi]^{\frac{N_s}{2}}}\frac{1}{\|\mathbf{C}_{\hat{\Psi}}\|^{\frac{1}{2}}}\exp\{-J(\hat{\Psi}_{N_s}, \Theta_{H_j})\} \tag{12}$$

Note that the search for the most likely damage hypothesis in Eq. (5) theoretically requires the examination of all possible damage scenarios. We have proposed a branch-and-bound search scheme using bounding heuristics to expedite this search without exhaustively examining all the possible damage hypotheses [17]. The following two pruning heuristics are employed in this study:

1. Let $H_j \cup D_i$ denote an extension of hypothesis $H_j$ by adding the $i$th substructure as damaged. If a posterior probability of $H_j \cup D_i$ is less than that of $H_j$, then further extension of $H_j \cup D_i$ is ruled out; i.e.

   $$\text{if } P(H_j \cup D_i|\hat{\Psi}_{N_s}) < P(H_j|\hat{\Psi}_{N_s}) \text{ stop extending } H_j \cup D_i \tag{13}$$

2. If a posterior probability of $H_j$ is less than $P_{\max}$ which is the largest posterior probability among all the hypotheses examined so far, then further extension of $H_j$ is ruled out; i.e.

   $$\text{if } P(H_j|\hat{\Psi}_{N_s}) < P_{\max}, \text{ stop extending } H_j \tag{14}$$

If the damages are localized in a few substructures, the number of damage hypotheses that need to be examined by the branch-and-bound search is relatively small and the search becomes computationally feasible.

### 2.2. Modification of the error function, $J(\hat{\Psi}_{N_s}, \Theta_{H_j})$

Previous works have suggested to select the appropriate modes which are sensitive to the critical members [4,12]. However, the ignorance of the actual damage locations hinders the selection scheme. Since the posterior probabilities of the assumed damage events are of interest in this Bayesian approach, the Ritz vectors, which are more sensitive to the stiffness changes of substructures in each assumed damage event, can be weighted for each case. In other words, the Ritz vectors, which are sensitive not to the unknown actual damage but to the assumed damage, can be

weighted for the computation of the error function. Realizing that $\mathbf{C}_{\hat{\Psi}}^{-1}$ in Eq. (7) is one form of weighting matrix, we modify the error function $J(\hat{\Psi}_{N_s}, \Theta_{H_j})$ such that each term of the error function is weighted considering the sensitivities of Ritz vectors to the assumed damage as well as the measurement uncertainties:

$$J(\hat{\Psi}_{N_s}, \Theta_{H_j}) = \frac{1}{2}\sum_{n=1}^{N_s} [\hat{\psi}(n) - \psi(\Theta_{H_j}) - e_M(\Theta_{H_o})]^T \mathbf{W}_r [\hat{\psi}(n) - \psi(\Theta_{H_j}) - e_M(\Theta_{H_o})] \quad (15)$$

where $\mathbf{W}_j$, is a diagonal matrix which weights each error term considering the uncertainty of measurements and the sensitivities of the corresponding $\boldsymbol{r}_{pk}$ to the assumed damage:

$$\mathbf{W}_r = \text{diag}[W_{\boldsymbol{r}_{11}}, W_{\boldsymbol{r}_{12}}, \ldots, W_{\boldsymbol{r}_{1N_d}}, W_{\boldsymbol{r}_{21}}, \ldots, W_{\boldsymbol{r}_{2N_d}}, \ldots, W_{\boldsymbol{r}_{N_r N_d}}] \quad (16)$$

In Eq. (16) $\boldsymbol{r}_{pk}$ denotes the $k$th component of the $p$th analytical Ritz vector and each diagonal entry $W_{\boldsymbol{r}_{pk}}$ is defined as follows:

$$W_{\boldsymbol{r}_{pk}}(\Theta_{H_j}) = \frac{w_{\boldsymbol{r}_{pk}}(\Theta_{H_j})}{\sigma^2_{\hat{\boldsymbol{r}}_{pk}}} \quad (17)$$

$w_{\boldsymbol{r}_{pk}}(\Theta_{H_j})$ weights the corresponding error term in Eq. (15) considering the sensitivity of $\boldsymbol{r}_{pk}$ to the assumed damage. $\sigma_{\hat{\boldsymbol{r}}_{pk}}$ is the standard deviation of the $k$th component of the $p$th estimated Ritz vector.

It should be noted that $\Theta_{H_j}$ contains all the information about the current damage state. The damaged substructures are the ones included in $H_j$ as damaged and the damage amount of the $i$th substructure, $\Delta\theta_j$, is $1 - \theta_j$. Since it is difficult to find the sensitivities of the Ritz vectors for multiple damage cases, we define the sensitivity of $\boldsymbol{r}_{pk}$ with respect to the current damage state as the rate of $\Delta\boldsymbol{r}_{pk}$ (the change of $\boldsymbol{r}_{pk}$ from the undamaged state) to the average change of $\theta_i (\in \Theta^1_{H_j})$. For simplicity, $\boldsymbol{r}_{pk}$ is assumed to change linearly with the change of $\theta_j$. Then, $\Delta\boldsymbol{r}_{pk}$ at the current damage state can be approximated as follows:

$$\Delta\boldsymbol{r}_{pk} \cong \sum_{\theta_i \in \Theta^1_{H_j}} \frac{\partial \boldsymbol{r}_{pk}}{\partial \theta_i} \Delta\theta_i \quad (18)$$

The sensitivity of $\boldsymbol{r}_{pk}$ at the current damage state, $S(\boldsymbol{r}_{pk}|\Theta_{H_j})$, is defined as:

$$S(\boldsymbol{r}_{pk}|\Theta_{H_j}) = \frac{\Delta\boldsymbol{r}_{pk}}{\Delta\bar{\theta}} \cong \sum_{\theta_i \in \Theta^1_{H_j}} \frac{\partial \boldsymbol{r}_{pk}}{\partial \theta_i} \frac{\Delta\theta_i}{\Delta\bar{\theta}} = \sum_{\theta_i \in \Theta^1_{H_j}} \frac{\partial \boldsymbol{r}_{pk}}{\partial \theta_i} \beta_i \quad (19)$$

where $\Delta\bar{\theta} = \frac{1}{N_{\theta^1}} \sum_{\theta_i \in \Theta^1_{H_j}} \Delta\theta_i, \beta_i = \frac{\Delta\theta_i}{\Delta\theta_i}$ and $N_{\theta^1}$ is the number of damaged substructures in a hypothesis $H_j$. The sensitivity of a Ritz vector is defined as:

$$S(\boldsymbol{r}_p|\Theta_{H_j}) = \frac{[\sum_{k=1}^{N} S^2(\boldsymbol{r}_{pk}|\Theta_{H_j})]^{\frac{1}{2}}}{[\sum_{k=1}^{N} r^2_{pk}(\Theta_{H_j})]^{\frac{1}{2}}} \quad (20)$$

where $N$ is the total number of DOFs in the analytical model. Finally, the weighting parameter $w_{\boldsymbol{r}_{pk}}(\Theta_{H_j})$ is related to $S(\boldsymbol{r}_p|\Theta_{H_j})$ as:

$$w_{\boldsymbol{r}_{pk}}(\Theta_{H_j}) = \frac{S(\boldsymbol{r}_p|\Theta_{H_j})}{\sum_{i=1}^{N_r} S(\boldsymbol{r}_i|\Theta_{H_j})} \text{ for all } k \quad (21)$$

### 2.3. Generation and sensitivity of Ritz vectors

The following introduces a generation procedure of Ritz vectors [14, 2], and the sensitivity of a Ritz vector with respect to the stiffness change of each substructure $\partial\boldsymbol{r}_p/\partial\theta_i$. Assume that the dynamic loading $\mathbf{F}$(s,t) can be separated into a spatial load vector $\boldsymbol{f}$(s) and a time function $u$(t):

$$\mathbf{F}(s,t) = \boldsymbol{f}(s)u(t) \quad (22)$$

then the first mass-normalized Ritz vector $\boldsymbol{r}_1$, is computed as:

$$\tilde{\boldsymbol{r}}_1 = \mathbf{K}^{-1}\boldsymbol{f}(s), \text{ and } \boldsymbol{r}_1 = \frac{\tilde{\boldsymbol{r}}_1}{[\tilde{\boldsymbol{r}}_1^T \mathbf{M} \tilde{\boldsymbol{r}}_1]^{\frac{1}{2}}} \quad (23)$$

Taking the product between the mass matrix and the previous Ritz vector $\mathbf{M}\boldsymbol{r}_{p-1}$ as a load, the recurrence relationship computes the next Ritz vector $\bar{\boldsymbol{r}}_p$:

$$\mathbf{K}\bar{\boldsymbol{r}}_p = \mathbf{M}\boldsymbol{r}_{p-1} : \text{ solve for } \bar{\boldsymbol{r}}_p \quad (24)$$

The linear independence of Ritz vectors is achieved using the Gram–Schmidt orthogonalization with respect to all the previous Ritz vectors:

$$\tilde{\boldsymbol{r}}_p = \bar{\boldsymbol{r}}_p - \sum_{q=1}^{p-1} (\boldsymbol{r}_q^T \mathbf{M} \bar{\boldsymbol{r}}_p)\boldsymbol{r}_q, \text{ and } \boldsymbol{r}_p = \frac{\tilde{\boldsymbol{r}}_p}{[\tilde{\boldsymbol{r}}_p^T \mathbf{M} \tilde{\boldsymbol{r}}_p]^{\frac{1}{2}}} \quad (25)$$

To compute the sensitivity of the $p$th Ritz vector with respect to the $i$th substructure stiffness $\partial\boldsymbol{r}_p/\partial\theta_i$, each step of the generation procedure of Ritz vectors is differentiated with respect to $\theta_j$. Taking the derivative on the first equation in Eq. (23) with respect to $\theta i$ gives:

$$\frac{\partial \bar{\boldsymbol{r}}_1}{\partial \theta_i} = -\mathbf{K}^{-1} \frac{\partial \mathbf{K}}{\partial \theta_i} \bar{\boldsymbol{r}}_1 \quad (26)$$

where $\partial\mathbf{K}/\partial\theta_i$ is computed by differentiating Eq. (1) with respect to $\theta_j$ and equal to the $i$th substructure stiffness $\mathbf{K}_j$. The second equation is differentiated in a similar manner to produce the sensitivity of the first Ritz vector:

$$\frac{\partial \boldsymbol{r}_1}{\partial \theta_i} = \frac{1}{[\tilde{\boldsymbol{r}}_1^T \mathbf{M} \tilde{\boldsymbol{r}}_1]^{\frac{1}{2}}} \frac{\partial \tilde{\boldsymbol{r}}_1}{\partial \theta_i} - \frac{[\tilde{\boldsymbol{r}}_1^T \mathbf{M} \frac{\partial \bar{\boldsymbol{r}}_1}{\partial \theta_i}]}{[\tilde{\boldsymbol{r}}_1^T \mathbf{M} \tilde{\boldsymbol{r}}_1]} \boldsymbol{r}_1 \quad (27)$$

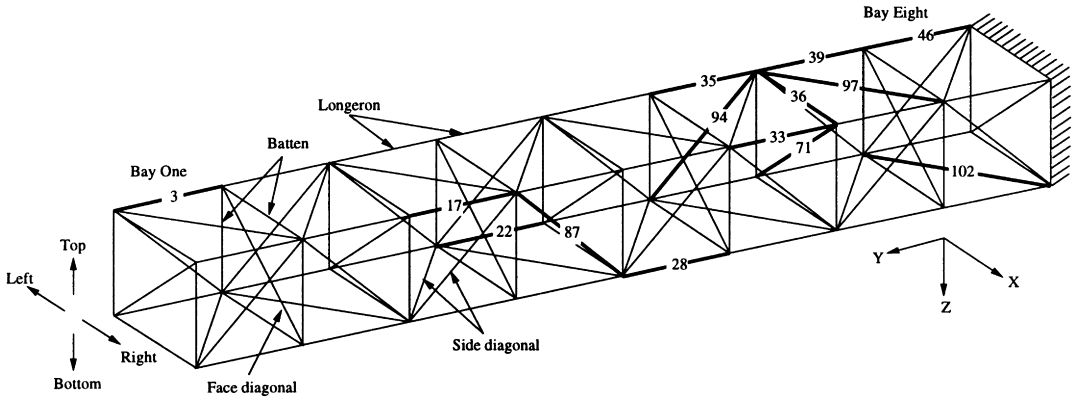


Fig. 1. An eight-bay truss structure.

The sensitivities of the additional Ritz vectors ($\boldsymbol{r}_p$: p ≠ 1) are computed in a similar manner by differentiating Eqs. (24) and (25) with respect to $\theta_j$:

$$\frac{\partial \bar{\boldsymbol{r}}_p}{\partial \theta_i} = \mathbf{K}^{-1}\left[ -\frac{\partial \mathbf{K}}{\partial \theta_i}\bar{\boldsymbol{r}}_p + \mathbf{M}\frac{\partial \boldsymbol{r}_{p-1}}{\partial \theta_i} \right] \tag{28}$$

$$\frac{\partial \tilde{\boldsymbol{r}}_p}{\partial \theta_i} = \frac{\partial \bar{\boldsymbol{r}}_p}{\partial \theta_i} - \sum_{q=1}^{p-1}\left[ \left( \frac{\partial \boldsymbol{r}_q^{\mathrm{T}}}{\partial \theta_i}\mathbf{M}\bar{\boldsymbol{r}}_p + r_q^{\mathrm{T}}\mathbf{M}\frac{\partial \bar{\boldsymbol{r}}_p}{\partial \theta_i} \right)\boldsymbol{r}_q + (\boldsymbol{r}_q^{\mathrm{T}}\mathbf{M}\bar{\boldsymbol{r}}_p)\frac{\partial \boldsymbol{r}_q}{\partial \theta_i} \right] \tag{29}$$

$$\frac{\partial \boldsymbol{r}_p}{\partial \theta_i} = \frac{1}{[\tilde{\boldsymbol{r}}_p^{\mathrm{T}}\mathbf{M}\tilde{\boldsymbol{r}}_p]^{\frac{1}{2}}}\frac{\partial \tilde{\boldsymbol{r}}_p}{\partial \theta_i} - \frac{[\tilde{\boldsymbol{r}}_p^{\mathrm{T}}\mathbf{M}\frac{\partial \bar{\boldsymbol{r}}_p}{\partial \theta_i}]}{[\tilde{\boldsymbol{r}}_p^{\mathrm{T}}\mathbf{M}\tilde{\boldsymbol{r}}_p]}\boldsymbol{r}_p \tag{30}$$

The derived sensitivity reveals how the sensitivity of a Ritz vector is related to that of the previous Ritz vectors. Further, the derivative in Eq. (30) is employed to calculate $S(\boldsymbol{r}_{pk}|\Theta_{H_j})$ in Eq. (19) and $w_{\boldsymbol{r}_{pk}}(\Theta_{H_j})$ in Eq. (21).

## 3. Numerical examples

This section demonstrates the potential applicability of Ritz vectors to damage detection of structures and the better sensitivity of Ritz vectors over the modal vectors. The first example structure is an eight-bay truss structure from the NASA dynamic scale model technology (DSMT) program of Langley Research Center [11]. The second example structure is a five-story frame building. This section is organized as follows. First, sensitivity analyses of Ritz vectors are conducted and the sensitivities of Ritz vectors are compared to those of modal vectors. Second, the damage detection of the eight-bay truss structure is conducted by changing damage locations and load patterns. Further, the damage detection using Ritz vectors is compared to the damage detection using modal parameters. Third, the proposed method is applied to the damage detection of the five-story frame building. The effect of the modeling error is highlighted in the frame structure example.

### 3.1. Sensitivity analyses of Ritz vectors

In this subsection, a sensitivity analysis of Ritz vectors is conducted using the eight-bay truss structure shown in Fig. 1. The structure is modeled using 104 truss elements, and consists of 36 nodes and 96 DOFs. In Fig. 1, the 36 nodes are numbered: (1) from the top left corner at the free end of the structure to the top right, bottom left and bottom right corner, respectively; and (2) from the bay one to the bay eight. The DOFs follow the node numbering and for each

Table 1
Classification of truss members into four lacing patterns. T, B, R and L denote top, bottom, right and left direction shown in Fig. 1, respectively

| Bay # | Longeron | | | | Batten | | | | Face diag. | Side diag. | | | |
|---|---|---|---|---|---|---|---|---|---|---|---|---|---|
| | TR | TL | BR | BL | T | B | R | L | | T | B | R | L |
| 1 | 5 | 3 | 4 | 7 | 1 | 2 | 50 | 49 | 65 | 74 | 76 | 73 | 75 |
| 2 | 9 | 11 | 13 | 10 | 6 | 8 | 51 | 52 | 66 | 77 | 80 | 79 | 78 |
| 3 | 17 | 15 | 16 | 19 | 12 | 14 | 54 | 53 | 67 | 81 | 84 | 82 | 83 |
| 4 | 21 | 23 | 25 | 22 | 18 | 20 | 55 | 56 | 68 | 85 | 88 | 87 | 86 |
| 5 | 29 | 27 | 28 | 31 | 24 | 26 | 58 | 57 | 69 | 89 | 92 | 90 | 91 |
| 6 | 33 | 35 | 37 | 34 | 30 | 32 | 59 | 60 | 70 | 93 | 96 | 95 | 94 |
| 7 | 41 | 39 | 40 | 43 | 36 | 38 | 62 | 61 | 71 | 97 | 100 | 98 | 99 |
| 8 | 47 | 46 | 45 | 48 | 42 | 44 | 63 | 64 | 72 | 103 | 102 | 101 | 104 |


Fig. 2. Load patterns applied to an eight-bay truss structure.

node, the DOFs are numbered consecutively the *x*, y, *z* translational DOFs.

Table 1 classifies the truss members into four different lacing patterns as shown in Fig. 1: longeron, batten, face diagonal and side diagonal. In the sensitivity analysis, load pattern 1 shown in Fig. 2(a) is employed for the generation of Ritz vectors.

The derived sensitivity is validated by comparing the analytical changes of Ritz vectors, computed using the derived sensitivity, with the actual changes of Ritz vectors. Figs. 3 and 4 present selected results for the comparison, where $\boldsymbol{r}_j^h$ and $\boldsymbol{r}_j^d$ represent the *j*th Ritz vector before and after the stiffness changes, respectively. Imposing load pattern 1 on the healthy structure, the first five successive Ritz vectors are generated from the procedures described in Eqs. (23)–(25). After decreasing the stiffness of each member by 1%, the actual changes of the Ritz vectors from the healthy state are computed to arrive at $\boldsymbol{r}_j^h - \boldsymbol{r}_j^d$. The corresponding analytical changes of the Ritz vectors are computed as $(\partial \boldsymbol{r}_j/\partial\theta_i) \times \Delta\theta_i$. Here $(\partial \boldsymbol{r}_j/\partial\theta_i)$ is the derived sensitivity from Eqs. (27)–(30) and $\Delta\theta_j$ is set to 0.01. As shown in Figs. 3 and 4, the analytical changes of the Ritz vectors, which are computed from the closed form sensitivity, are in good agreement with the actual changes of the Ritz vectors.

Next, the sensitivities of Ritz vectors are compared to the sensitivities of modal vectors. The comparison of the first five Ritz and modal vectors, as shown in Fig. 5, reveals that the Ritz vectors, particularly the higher Ritz vectors, produce more complicated deformed shapes. This implies intuitively that Ritz vectors might be more sensitive to the stiffness changes of substructures. This observation can be justified by a detailed sensitivity analysis. The sensitivity analysis is conducted by comparing the changes of the Ritz and modal vectors as the stiffness of each substructure (member) deteriorates. Selected results from the comparisons are presented in Fig. 6 where the stiffness loss of the selected member varies from 0% to 100%. Here, $\|\cdot\|$ denotes the Euclidean norm, $\boldsymbol{r}^h$ and $\mathbf{r}^{\mathrm{d}}$ denote the Ritz vectors before and after damage occurs, respectively, and $\boldsymbol{v}^h$ and $\mathbf{v}^{\mathrm{d}}$ present the modal vectors before and after stiffness changes, respectively. The shaded portion of Fig. 6(a) indicates that if each component of a modal vector has a 5% uncertainty, no measurable change in any modal vector will be apparent unless the stiffness loss exceeds 75%. On the other hand, 10% change of stiffness results in perceivable changes in the second and third Ritz vectors in the presence of a 5% uncertainty.

From the sensitivity analyses, several observations can be made in this example: (1) in most cases, stiffness changes in the model lead to larger changes in the Ritz vectors than in the modal vectors; (2) face diagonals do not cause significant changes to either the Ritz or modal vectors; and (3) in many cases, Ritz and modal vectors are more sensitive to the stiffness losses of side diagonals and longerons than those of battens. The sensitivity analyses allow one to determine detectable damage amounts for each substructure before the actual damage detection. Detectable damage should cause significant changes of Ritz vectors greater than what can be attributed to measurement uncertainties, modeling error or environmental effects.

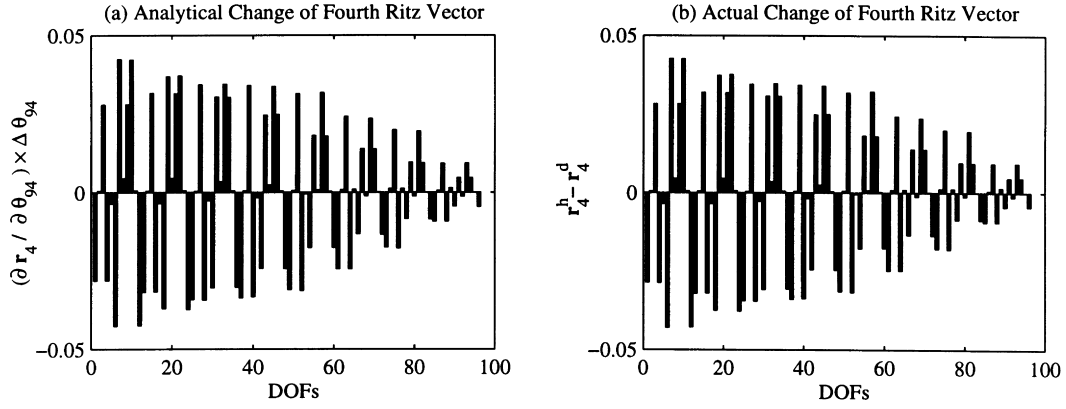


Fig. 3. Change of the fourth Ritz vector caused by a 1% decrease of the 94th member stiffness.

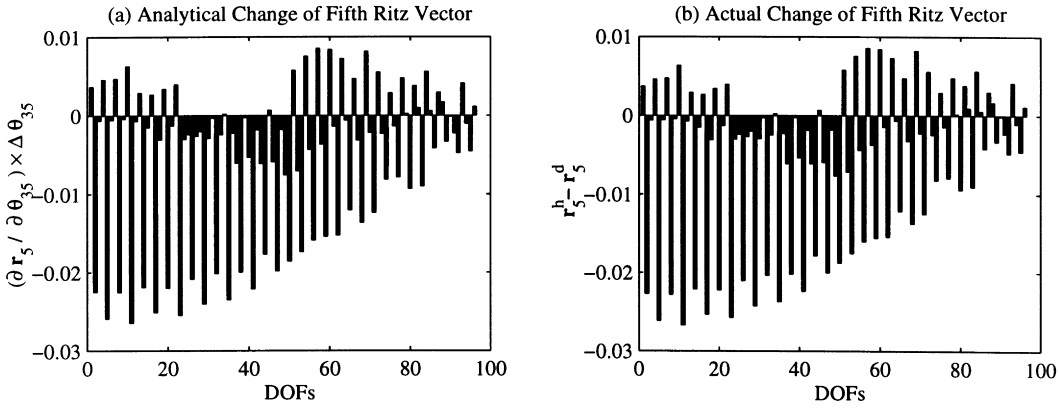


Fig. 4. Change of the fifth Ritz vector caused by a 1% decrease of the 35th member stiffness.

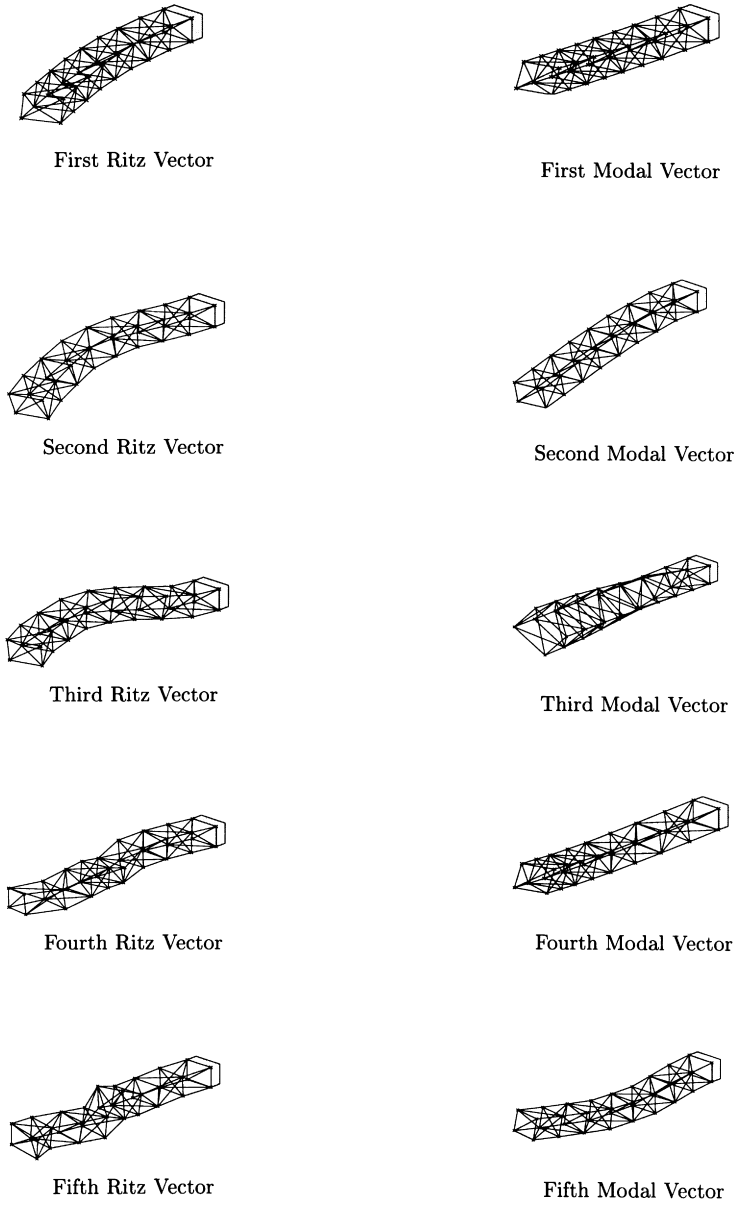


Fig. 5. Comparison of Ritz vectors and modal vectors of an eight-bay truss structure.

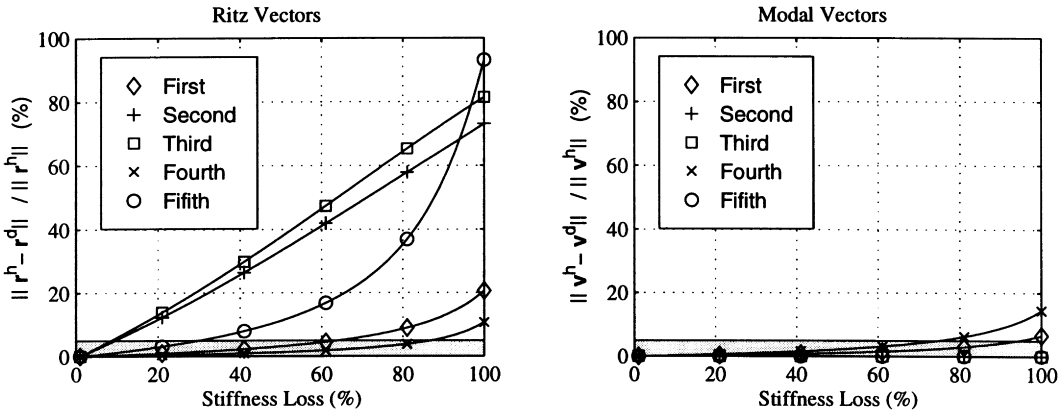


(a) Progressive damage in member 33 (a longeron in bay 6)

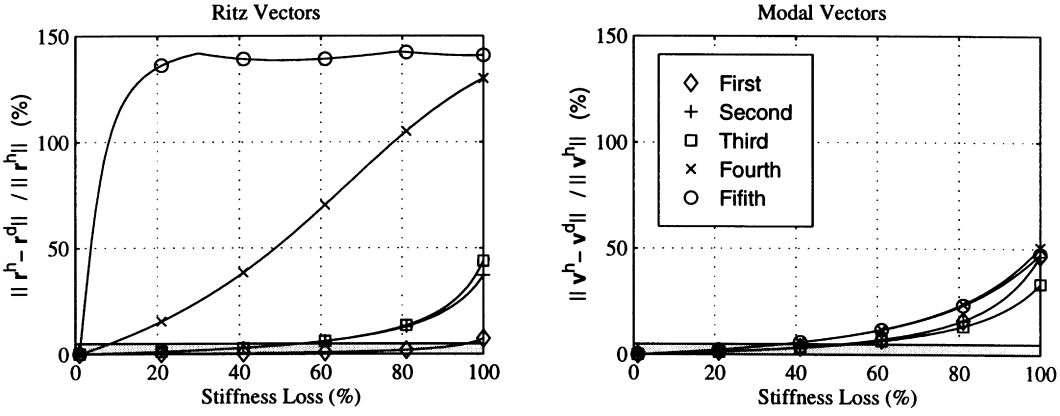


(b) Progressive damage in member 94 (a side diagonal in bay 6)

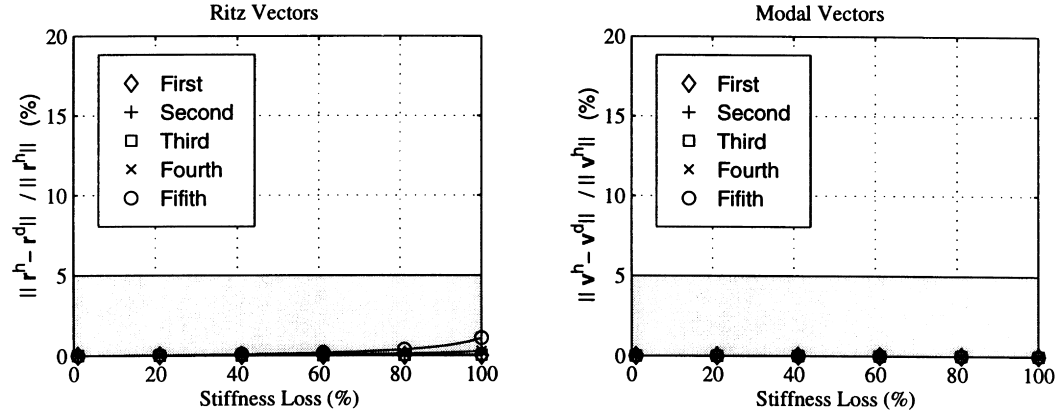


(c) Progressive damage in member 71 (a face diagonal in bay 7)

Fig. 6. Sensitivity comparison of Ritz and modal vectors for an eight-bay truss structure.

### *3.2. Damage detection of an eight-bay truss structure*

This subsection presents the diagnosis results of an eight-bay truss structure conducted under different conditions. For all examples, a uniform prior probability is assigned to all hypotheses. Therefore, the determination of the most probable hypothesis in Eq. (6) depends only on the error function $J(\hat{\Psi}_{N_s}, \Theta_{H_j}^{\max})$. The search space $\Theta_{H_j}\Omega_{H_j}^{*}$ in Eq. (11) is

Table 2
Minimum detectable damage amount of each substructure for a given load pattern. "—" denotes that damage is undetectable

| | Bay # | Sub. # | Load pattern | | | Modal vector | Sub. # | Load Pattern | | | Modal vector |
|---|---|---|---|---|---|---|---|---|---|---|---|
| | | | (1) | (2) | (3) | | | (1) | (2) | (3) | |
| Longeron | 1 | 3 | 50% | 10% | 90% | 80% | 5 | 70% | — | 40% | 100 |
| | | 4 | 50% | 20% | 70% | 80% | 7 | 70% | — | 90% | 100% |
| | 2 | 9 | 10% | 20% | 60% | 60% | 11 | 40% | 10% | 90% | 80% |
| | | 10 | 10% | 20% | 60% | 60% | 13 | 40% | 20% | 70% | 80% |
| | 3 | 15 | 30% | 10% | 40% | 50% | 17 | 10% | 20% | 60% | 60% |
| | | 16 | 30% | 10% | 30% | 50% | 19 | 10% | 20% | 50% | 60% |
| | 4 | 21 | 10% | 10% | 20% | 60% | 23 | 20% | 10% | 40% | 50% |
| | | 22 | 20% | 10% | 20% | 60% | 25 | 20% | 10% | 30% | 50% |
| | 5 | 27 | 10% | 10% | 10% | 60% | 29 | 10% | 10% | 20% | 50% |
| | | 28 | 10% | 10% | 10% | 50% | 31 | 20% | 10% | 20% | 50% |
| | 6 | 33 | 10% | 10% | 10% | 80% | 35 | 10% | 10% | 10% | 50% |
| | | 34 | 10% | 10% | 10% | 80% | 37 | 10% | 10% | 10% | 50% |
| | 7 | 39 | 10% | 10% | 10% | 80% | 41 | 10% | 10% | 10% | 80% |
| | | 40 | 10% | 10% | 10% | 70% | 43 | 10% | 10% | 10% | 80% |
| | 8 | 45 | 10% | 10% | 10% | 70% | 47 | 10% | 10% | 10% | 60% |
| | | 46 | 10% | 10% | 10% | 70% | 48 | 10% | 10% | 10% | 60% |
| Batten | 1 | 1 | 40% | 20% | 90% | 100% | 49 | 40% | 10% | 90% | 100% |
| | | 2 | 10% | 10% | 80% | 100% | 50 | 40% | 10% | 60% | 100% |
| | 2 | 6 | 30% | 60% | — | — | 51 | 40% | 50% | 90% | — |
| | | 8 | 40% | 60% | — | — | 52 | 60% | 50% | — | — |
| | 3 | 12 | 30% | 100% | 100% | — | 53 | 80% | 90% | 100% | — |
| | | 14 | 30% | 100% | 100% | — | 54 | 70% | 90% | 90% | — |
| | 4 | 18 | 30% | 70% | 100% | — | 55 | 70% | 60% | — | — |
| | | 20 | 40% | 70% | 100% | — | 56 | 60% | 70% | 100% | — |
| | 5 | 24 | 50% | 30% | — | — | 57 | 10% | 20% | 100% | — |
| | | 26 | 40% | 30% | — | — | 58 | 40% | 30% | 100% | — |
| | 6 | 30 | 50% | 80% | 10% | 100% | 59 | 60% | 70% | — | 100% |
| | | 32 | 60% | 80% | 90% | 100% | 60 | 60% | 70% | 10% | 100% |
| | 7 | 36 | 70% | 80% | 10% | — | 61 | 80% | 90% | 10% | — |
| | | 38 | 70% | 80% | 90% | — | 62 | 80% | 90% | 10% | — |
| | 8 | 42 | 90% | 100% | 70% | — | 63 | 90% | 90% | 80% | — |
| | | 44 | 90% | 100% | 60% | — | 64 | 90% | 90% | 70% | — |
| Side diagonal | 1 | 73 | 10% | 10% | 40% | 70% | 75 | 10% | 10% | 90% | 70% |
| | | 74 | 10% | 10% | 80% | 70% | 76 | 10% | 10% | 70% | 70% |
| | 2 | 77 | 10% | 10% | 80% | 60% | 79 | 10% | 10% | 60% | 60% |
| | | 78 | 10% | 10% | 70% | 60% | 80 | 10% | 10% | 70% | 60% |
| | 3 | 81 | 10% | 10% | 70% | 60% | 83 | 10% | 10% | 70% | 60% |
| | | 82 | 10% | 10% | 70% | 60% | 84 | 10% | 10% | 60% | 60% |
| | 4 | 85 | 10% | 10% | 70% | 60% | 87 | 10% | 10% | 70% | 60% |
| | | 86 | 10% | 10% | 60% | 60% | 88 | 10% | 10% | 60% | 60% |
| | 5 | 89 | 10% | 10% | 60% | 60% | 91 | 10% | 10% | 60% | 60% |
| | | 90 | 10% | 10% | 60% | 60% | 92 | 10% | 10% | 60% | 60% |
| | 6 | 93 | 10% | 10% | 50% | 40% | 95 | 10% | 10% | 50% | 40% |
| | | 94 | 10% | 10% | 60% | 40% | 96 | 10% | 10% | 50% | 40% |
| | 7 | 97 | 10% | 10% | 40% | 20% | 99 | 10% | 10% | 50% | 20% |
| | | 98 | 10% | 10% | 40% | 20% | 100 | 10% | 10% | 40% | 20% |
| | 8 | 101 | 10% | 10% | 30% | 20% | 103 | 10% | 10% | 40% | 20% |
| | | 102 | 10% | 10% | 20% | 20% | 104 | 10% | 10% | 30% | 20% |
| Face diagonal | 1,2 | 65 | 80% | 20% | 30% | — | 66 | — | 90% | 30% | — |
| | 3,4 | 67 | — | — | 30% | — | 68 | — | 100% | 30% | — |
| | 5,6 | 69 | 80% | 30% | 30% | — | 70 | — | 100% | 30% | — |
| | 7,8 | 71 | — | — | 30% | — | 72 | — | — | 40% | — |

Table 3
Comparison of diagnosis results using Ritz or modal vectors. $N_s = 1$, noise = 5%, and all DOFs are measured. Only longeron and side diagonal members are examined for damage

| Case | Actual Damage | | Rank[a] | | |
|---|---|---|---|---|---|
| | $L_{dam}$ | $D_{dam}$ | scheme 1[b] | scheme 2[c] | scheme 3[d] |
| A | {46} | {10%} | 3/313 | 3/313 | 350/434 |
| B | {102} | {10%} | 1/251 | 4/374 | 30/434 |
| C | {39} | {10%} | 3/313 | 6/313 | 350/434 |
| D | {97} | {10%} | 3/313 | 3/313 | 55/434 |
| G | {33} | {10%} | 2/313 | 3/313 | 372/434 |
| H | {35} | {10%} | 3/313 | 3/313 | 219/434 |
| I | {94} | {10%} | 3/313 | 3/313 | 356/434 |
| J | {28} | {10%} | 3/313 | 7/374 | 382/434 |
| K | {87} | {10%} | 1/251 | 3/313 | 405/434 |
| L | {22} | {10%} | 3/313 | 4/374 | 320/434 |
| M | {17} | {10%} | 3/313 | 3/252 | 428/494 |
| N | {13} | {10%} | 3/313 | 3/313 | 213/494 |

[a] The first number is the rank of the actual damage event and the second is the total number of the examined hypotheses.
[b] The first five Ritz vectors are estimated from load pattern 2 and the proposed weighting scheme is employed.
[c] Same as scheme 1 except that the weighting scheme is not used.
[d] The first five modal vectors are employed instead of Ritz vectors.

evaluated at the intersection of grid lines which discretize the search domain with an increment of $\Delta\theta$. For all numerical examples, we use an incremental step $\Delta\theta = 0.1$. The branch-and-bound search in the presented examples follows a depth-first/best-first search strategy. Furthermore, the extension of the branch-and-bound search is limited such that a maximum of three substructures can be examined.

Each Ritz vector is normalized with respect to the DOF which has the absolute maximum magnitude in the healthy structure. Since one component is used for normalization, only $N_r - 1$ pieces of information exist for each Ritz vector. To simulate the estimated Ritz vectors $\hat{\psi}$, the Ritz vectors $\psi$ obtained from Eqs. (23)–(25) are perturbed with noise such that:

$$\hat{\psi}(n) = \psi\left(1 + \frac{\mathcal{N}}{100}\mathcal{R}\right) \tag{31}$$

where $\mathcal{N}$ is a specified percentage of noise level, and $\mathcal{R}$ is a normally distributed random number with zero mean and a variance of 1.0. This process is repeated $N_s$, times to simulate the $N_s$, data sets.

Excitation is assumed to be a swept sine excitation generated from electrodynamics or hydraulic shakers [5]. All actuators are assumed to generate forces with the same magnitude and phase. According to Eq. (22), the spatial distribution of forces is defined by a vector $\boldsymbol{f}(s)$ and an identical input excitation is given to all actuators by a scalar function $u(t)$. Load patterns are selected to maximize the sensitivities of the first five Ritz vectors over all substructures. For all examples, $L_{dam}$ and $D_{dam}$, denote the actual damage locations and the associated damage amount, respectively. $\hat{L}_{dam}$ and $\hat{D}_{dam}$ denote the most probable damage locations and the associated damage amount estimated by the proposed method. In addition, the measured DOFs and the estimated modes are denoted by DOFm and MODEm, respectively.

### 3.2.1. Diagnoses using uniform damage thresholds

In this subsection, twelve different damage cases are investigated employing Ritz vectors and the proposed weighting scheme. For the purpose of comparison, the same damage cases are re-diagnosed using Ritz vectors but without the weighting scheme. Furthermore, the diagnosis results using modal vectors are presented. Sensitivity analyses which are similar to Fig. 6 are conducted for load patterns 1 and 2 to compute a minimum detectable damage. The minimum detectable damage of each substructure is defined as the minimum damage amount for which the estimated Ritz vectors from a given load pattern can detect when each component of a Ritz vector is contaminated by a certain level of noise. The minimum detectable damage of each substructure is presented in Table 2 assuming that, because of noise, each component of a Ritz vector is perturbed by 5% of its magnitude.

Table 2 shows that a stiffness loss larger than 10% is detectable from load patterns 1 and 2 for most side diagonals and longerons. Battens undergo a 10%–100% loss of stiffness before the changes of Ritz vectors become observable. However, the stiffness changes of most face diagonals are undetectable from both load patterns. Based on these preliminary sensitivity analyses, the detection of 10% stiffness loss in most face diagonals and battens seems difficult from the assumed load patterns. Therefore, the face diagonals and battens are precluded from the branch-and-bound search in the examples presented here. That is, only longerons and side diagonals are investigated for potential damage. As shown in Table 2, the Ritz vectors are clearly more sensitive to damage than the modal vectors. For load pattern 3, 16 actuators are assumed to be placed at both ends of all face diagonals to produce tensile forces in the face diagonals. This load pattern is presented here to show that this load pattern can make the face diagonals more detectable (larger than 30% stiffness loss is detectable from the Ritz vectors generated from load pattern 3). However, since this loading is not realistic, only the first two load patterns are employed for damage detection.

Twelve damage cases with a single damaged substructure are simulated by assuming a 10% stiffness loss, a 5% noise level and one data set ($N_s = 1$). The damaged substructures used in the examples are shown in Fig. 1 by solid lines. Furthermore, all DOFs are assumed to be measured and a value of 0.9 is used for the damage threshold $\theta^*$ of each substructure. The damage locations are identical to some of the damage cases which are experimentally tested and described in Kashangaki [11]. It should be noted that while the damage cases in Kashangaki [11] refer to the total removal of a truss member, only a 10% stiffness loss is considered in this study.

Table 4
Diagnoses of an eight-bay truss structure using different threshold values. The first five Ritz vectors are estimated from load pattern 2 and the proposed weighting scheme is employed. $N_s = l$, noise = 5%, and all DOFs are measured. Different damage threshold value is assigned to each substructure

| Case | Actual damage | | Rank[a] | Most prob. damage | |
|---|---|---|---|---|---|
| | $L_{dam}$ | $D_{dam}$ | | $\hat{L}_{dam}$ | $\hat{D}_{dam}$ |
| A | {46} | {10%} | 1/371 | {46} | {10%} |
| B | {102} | {10%} | 1/552 | {102} | {10%} |
| C | {39} | {10%} | 1/371 | {39} | {10%} |
| D | {97} | {10%} | 1/461 | {97} | {10%} |
| E | {36} | {10%} | 17/95 | No damage | |
| F | {71} | {10%} | –/95 | No damage | |
| G | {33} | {10%} | 1/371 | {33} | {10%} |
| H | {35} | {10%} | 1/461 | {35} | {10%} |
| I | {94} | {10%} | 1/462 | {94} | {10%} |
| J | {28} | {10%} | 1/371 | {28} | {10%} |
| K | {87} | {10%} | 1/371 | {87} | {10%} |
| L | {22} | {10%} | 1/461 | {22} | {10%} |
| M | {17} | {10%} | 9/95 | No damage | |
| N | {3} | {10%} | 1/461 | {3} | {10%} |

[a] The first number is the rank of the actual damage event and the second is the total number of the examined hypotheses. "–" denotes that actual damage is not detected.

Table 3 shows the diagnosis results of the twelve damage cases. Scheme 1 uses the first five Ritz vectors and the proposed weighting and scheme 2 uses the same Ritz vectors without the weighting scheme. These Ritz vectors are generated from load pattern 2. In scheme 3, the first five modal vectors are employed instead of the Ritz vectors. Table 3 shows that scheme 1 provides the best diagnoses among the three schemes. For all damage cases, the most probable damage event computed by scheme 1 includes the actually damaged substructure. In some cases, however, undamaged substructures are found to be included in the most probable damage event. For example, the 7th substructure is included as a potentially damaged substructure in case A. Table 2 shows that the Ritz vectors employed in this diagnosis set (the Ritz vectors generated from load pattern 2) are insensitive to the stiffness changes of the 7th substructure. Therefore, a small stiffness change of the 7th substructure may not result in a noticeable change of the error function value in Eq. (7) or can actually reduce the error function value when Ritz vectors are noise contaminated. For similar reasons, the 5th substructure is also included in the most probable damage event for other damage cases. Comparing schemes 1 and 2, we observe that the weighting in scheme 1 slightly improves the diagnoses. Scheme 3 using modal vectors fails to detect most damage cases. These results show the superiority of Ritz vectors to modal vectors for damage detection.

Table 5
Diagnoses of an eight-bay truss structure with multiple damage locations. $N_s = l$, noise = 5%, all DOFs are measured and the proposed weighting scheme is employed. Different damage threshold value is assigned to each substructure

| Case | Actual damage | | Rank[a] | | |
|---|---|---|---|---|---|
| | $L_{dam}$ | $D_{dam}$ | F1[b] | F2[c] | F1, F2[d] |
| O | {35,94} | {10%,10%} | 1/672 | –/371 | 1/686 |
| P | {39,46} | {10%,10%} | 1/483 | 1/644 | 1/686 |
| Q | {28,102} | {10%,10%} | 1/861 | 2/914 | 1/974 |
| R | {39,87} | {10%,10%} | –/672 | 1/644 | 1/679 |
| S | {22,35,97} | {10%,10%,10%} | –/672 | –/644 | 1/686 |
| T | {17,35,97} | {10%,10%,10%} | 1/577 | –/554 | 1/986 |

[a] The first number is the rank of the actual damage event and the second is the total number of the examined hypotheses. "–" denotes that actual damage is not detected.
[b] The first five Ritz vectors are estimated from load pattern 1.
[c] The first five Ritz vectors are estimated from load pattern 2.
[d] Load Patterns 1 and 2 are employed and the first five Ritz vectors are estimated from each load pattern (i.e. a total of ten Ritz vectors).

### 3.2.2. Diagnoses using different damage thresholds

In this subsection, fourteen damage cases (including the previous twelve cases) are diagnosed using a different threshold value for each substructure. The other conditions are unchanged (noise = 5%, $N_s = 1$ and all DOFs are measured). We prevent unnecessary extensions of the branch-and-bound search by employing preliminary sensitivity analyses The branch-and-bound search is conducted including only substructures with damage larger or equal to the pre-assigned minimum detectable damage.

The damage thresholds in this subsection are assigned based on the minimum detectable damage computed in Table 2. For example, since the minimum detectable damage amount assigned to the first substructure is 20% (when load pattern 2 is employed), the corresponding damage threshold is set to 0.8 (1 − 0.2). The damage thresholds for other substructures are determined in the same fashion. It should be noted that when the total removal of a substructure does not cause a perceivable change in Ritz vectors, the substructure is defined as undetectable and excluded from the diagnosis. For example, the 67th member is defined as undetectable since the total removal of the member (100% stiffness loss) does not yield significant changes in Ritz vectors beyond the assumed variation caused by uncertainties. Therefore, the 67th member is excluded from the diagnosis.

Table 4 shows that the redefined damage threshold improves the diagnoses. Comparing the most probable events (hypothesis) of case A in Tables 3 and 4, one can observe that the undamaged 7th substructure is removed from the most probable hypothesis, making the actual damage case the most probable one. In case E, the proposed method indicates that most likely there is no damage. Considering the fact that the damage threshold of the 36th substructure is set to 0.2, the 10% stiffness loss in the 36th substructure is not detectable. The proposed method ranks the 36th substructure as the 17th most probable damage location with 80% damage. Similar results are observed

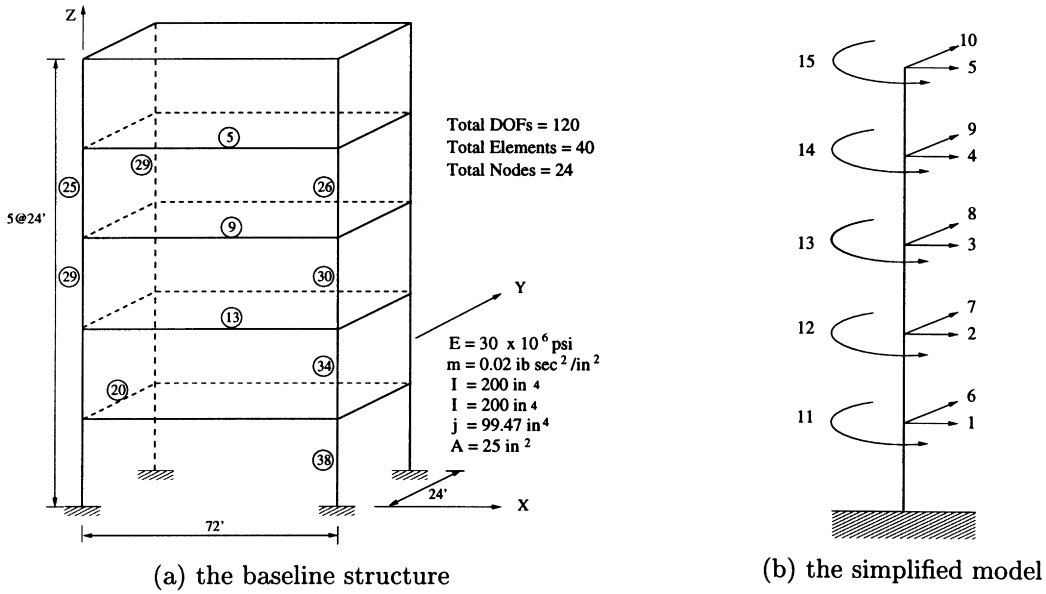


Fig. 7. The baseline structure and the simplified model of a five-story frame structure.

for cases F and M. Sensitivity analyses in Table 2 show that the stiffness deterioration of the 71th substructure, which is a face diagonal in the seventh-bay, does not yield any noticeable changes to the estimated Ritz vectors. Therefore, the 71th substructure is precluded from the diagnosis and the proposed method provides a false-negative indication of damage. For case M, the damage threshold of the 17th substructure is set to 0.8. Again, the proposed method indicates that most likely there is no damage and ranks the event of 20% damage in the 17th substructure as the 9th most probable damage case.

### *3.2.3. Diagnoses of damage in multiple locations*

In this subsection, we focus on the detection of damage in multiple locations. Table 5 presents diagnosis results of six different damage cases. In cases O–R, a 10% stiffness decrease is simulated in two substructures. Cases S and T present damage cases with three damaged substructures. The six damage cases are repeatedly diagnosed under different conditions. In the fourth column of Table 5, the first five Ritz vectors are generated from load pattern 1 and employed for damage detection along with the proposed weighting scheme. In the fifth column, load pattern 2 is employed instead of load pattern 1. In the last column of the table, a total of ten Ritz vectors are generated from load patterns 1 and 2 (the first five Ritz vectors are generated from each load pattern). For all cases in Table 5, all DOFs are measured and one set of Ritz vectors is simulated assuming a 5% noise level ($N_s = 1$ and noise = 5%). Furthermore, the proposed weighting scheme is employed.

When the first five Ritz vectors are generated from load pattern 1, the proposed method identifies the actual damage event of cases O, P, Q and T. However, the actual damage locations are not detected for cases R and S. While the use of load pattern 2 yields the detection of actual damage locations in cases P, Q and R, load pattern 2 fails to identify damage of cases O, S and T. Finally, when a total of ten Ritz vectors are generated from load patterns 1 and 2, the proposed method identifies the actual damage locations for all cases (cases O–T). It is shown that each damage case has different sensitivity to different load patterns and by including more Ritz vectors from different load patterns, diagnosis results can be improved.

### *3.3. Damage detection of a five-story three-dimensional frame structure*

A five-story three-dimensional frame structure is employed to illustrate the applicability of Ritz vectors to damage detection when differences exist between the baseline structure and the simplified model. The term *baseline structure* is used to refer to a structure from which the experimental Ritz vectors are simulated. The simplified model is constructed such that the system stiffness matrix of the three-dimensional structure is obtained by assembling the lateral stiffness matrices of the planar frames [17]. Fig. 7 (a) and (b) show the baseline structure and the simplified model, respectively. While the baseline FE model has 6 DOFs at each node (three translational and three rotational DOFs), the simplified model has only three DOFs at the mass center of each floor. For the current five-story example, the baseline structure has 120 DOFs and the simplified model has 15 DOFs.

In many vibration tests of building structures, displacements are evaluated at the mass center of the floor diaphragm. Assuming a kinematic constraint that each floor diaphragm is rigid in its own plane, the deformation of the FE model is reconstructed at the mass center of every

Table 6
Diagnoses of a five-story frame structure considering modeling error. The first six Ritz vectors are estimated from load pattern 1 in Fig. 8. $N_s = 1$ and noise = 5%. The damage threshold is set to 0.9 for all substructures

| Case | Actual damage | | Rank[a] | Most prob. damage | |
|---|---|---|---|---|---|
| | $L_{dam}$ | $D_{dam}$ | | $\hat{L}_{dam}$ | $\hat{D}_{dam}$ |
| A | {5} | {10%,10%} | 51/266 | {5,25} | {10%,10%} |
| B | {5,9} | {10%,10%} | 8/266 | {5,9,25} | {10%,10%,10%} |
| C | {13,20} | {10%,10%} | 1/303 | {13,20} | {10%,10%} |
| D | {25,28} | {10%,10%} | 1/193 | {25,28} | {10%,10%} |
| E | {25,30} | {10%,10%} | 1/266 | {25,30} | {20%,10%} |
| F | {9,25} | {10%,10%} | 2/266 | {9,25,28} | {10%,10%,10%} |
| G | {34,38} | {10%,10%} | 1/266 | {34,38} | {10%,10%} |
| H | {26,29} | {10%,10%} | 7/230 | {25,26,29} | {10%,10%,10%} |

[a] The first number is the rank of the actual damage event and the second is examined hypotheses.

floor to simulate the real testing conditions. Then, the components of the estimated Ritz vector coincide with those of the simplified model. Loads applied to the baseline structure are also converted to equivalent forces in the simplified model using the displacement transformation matrix which relates the DOFs of the baseline structure to the mass center DOFs of the simplified model. Furthermore, for the calculation of $e_M(\Theta_{H_o})$ in Eq. (9), $\hat{\psi}_m^h$ is computed from the Ritz vectors of the initial FE model without damage. $\psi(\Theta_{H_o})$ is obtained from the simplified model following Eqs. (23)–(25). That is, $e_M(\Theta_{H_o})$ is defined as an output error caused by the difference between the baseline structure and the simplified model.

The first six Ritz vectors are estimated from each load pattern. Since the frame example in this subsection has less redundancy and the estimated Ritz vectors are reasonably sensitive to all substructures, the damage threshold is set to 0.9 for every substructure.

### 3.3.1. Diagnoses of damage cases with modeling error

The applicability of the proposed method is illustrated when a modeling error exists between the baseline structure and the simplified model. To highlight the effect of a modeling error, the effect of measurement noise is neglected in this example. Table 6 summarizes the diagnoses of eight different damage cases using the first six Ritz vectors generated from load pattern 1 and only one set of them is simulated ($N_s = 1$). Load pattern 1 and the other load patterns employed in the next example are presented in Fig. 8. The damaged substructures in Table 6 are shown as circled numbers in Fig. 7. Each beam and column in the baseline structure is modeled as a substructure, and altogether, the system consists of 40 substructures. Since the stiffness matrix of the simplified system is represented as an assembly of the effective stiffness contribution of each substructure (see Sohn and Law [17]), damage locations can be tracked at the substructure level of the baseline structure. That is, damage locations are identified in the baseline structure, not in the simplified model.

For cases C, D, E and G of Table 6, the proposed method ranks the actual damage event as the most likely damage event. In cases A, B, F and H, the actual damage locations are included in the most probable damage event, which the proposed method identifies. However, undamaged substructures are also mistakenly included in this most probable damage event. For example, in case B, the proposed method diagnoses that damage is most likely located in the 5th, 9th and 25th substructures. While the 5th and 9th substructures are actually damaged, the 25th substructure is mistakenly included. This can be explained as follows. We search for the most likely hypothesis $H_{\max}$ and the corresponding nondimensional parameter value $\Theta_{H_{\max}}^{\max}$ which minimizes the approximated error function $J(\hat{\Psi}_{N_s}, \Theta_{H_j})$ defined in Eq. (6). For the exact definition of $J(\hat{\Psi}_{N_s}, \Theta_{H_j})$, $e_M(\Theta_{H_d})$, which is the output error caused by the modeling error after damage occurrence, should be evaluated. Since the actual damage locations and amount, which are required to evaluate $e_M(\Theta_{H_d})$, are unknown, $e_M(\Theta_{H_d})$ is approximated by $e_M(\Theta_{H_o})$. Here, $e_M(\Theta_{H_o})$ is the output error caused by the modeling error before damage occurrence, assuming that the modeling error is constant for arbitrary damage locations and damage amount. Since Ritz vectors are very sensitive to stiffness changes, it appears that a relatively large difference between $e_M(\Theta_{H_d})$ and $e_M(\Theta_{H_o})$ may exist even for the small damage amount like the 10% stiffness loss presented in the example here. This difference explains why the undamaged substructures are mistakenly included in the most probable damage event in cases A, B, F and F, and why the estimated damage amount is slightly different from the actual damage amount in case E. However, using the simplification technique, we are able to reduce the size of the system from 120 DOFs to 15 DOFs without losing significant accuracy.

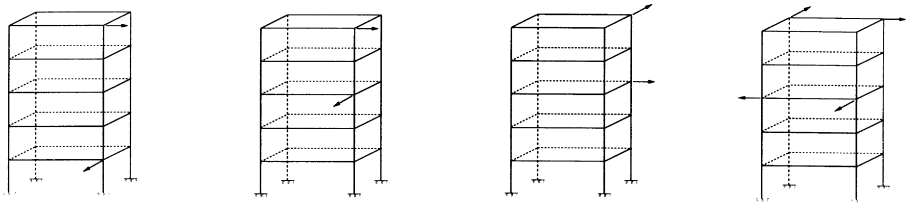

(a) Load pattern 1 (b) Load pattern 2 (c) Load pattern 3 (d) Load pattern 4

Fig. 8. Load patterns applied to a five-story frame structure.

Table 7
Diagnoses of a five-story frame structure using different load patterns

| Case[a] | The rank of the actual damage event[b] | | | | | |
|---|---|---|---|---|---|---|
| | F1[c] | F2 | F3 | F4 | MV[d] | All F's[e] |
| A | 51/266 | 3/230 | 3/230 | 18/255 | 32/266 | 1/155 |
| B | 8/266 | 3/266 | 7/266 | 15/266 | 20/266 | 6/266 |
| C | 1/303 | 2/266 | 1/375 | 5/155 | 100/193 | 1/230 |
| D | 1/193 | 1/230 | 1/193 | 14/230 | –/155 | 2/155 |
| E | 1/266 | 4/266 | –/41 | 2/337 | –/41 | 1/266 |
| F | 2/266 | 2/266 | 1/266 | 2/266 | –/80 | 1/302 |
| G | 1/266 | 1/267 | 2/303 | 1/303 | 5/266 | 1/267 |
| H | 7/230 | –/41 | 3/266 | 2/338 | –/41 | 1/302 |

[a] The damage cases here are identical to the damage cases in Table 6.
[b] The first number is the rank of the actual damage event and the second is the total number of the examined hypotheses. "–" denotes that actual damage event is not detected.
[c] In Fl, F2, F3 and F4, the first six Ritz vectors are estimated from load patterns 1, 2, 3 and 4, respectively.
[d] In MV, the first six modal vectors are estimated.
[e] Load patterns 1–4 are employed and the first six Ritz vectors are generated from each load pattern.

The eight damage cases are re-diagnosed in Table 7 employing four different load patterns and a combination of them. Except changing the load patterns, all the other conditions remain the same as the cases shown in Table 6. Table 7 shows that a careful selection of load patterns can improve diagnoses of damage and, in general, Ritz vectors provide better diagnoses than modal vectors. For example, by imposing load pattern 1 on the frame structure, the proposed method identifies the actual damage locations in four out of eight cases (cases C, D, E and G). Even for the other four cases (cases A, B, F and H), all the actual damage locations are included in the most probable damage event. Load pattern 2 fails to detect the actual damage event in case H, load pattern 3 does not find the actual damage event of case E, and load pattern 4 ranks the actual damage event as the most probable one only for case G. When all four load patterns are employed simultaneously (the last column of Table 7), the rank of the actual damage event is improved for most damage cases.

Table 8
Diagnoses of a frame structure considering modeling error and measurement noise

| Case[a] | The rank of the actual damage event[b] | | | | Most prob. damage[c] | |
|---|---|---|---|---|---|---|
| | $N_s = 1$ | $N_s = 5$ | $N_s = 10$ | $N_s = 20$ | $\hat{L}_{dam}$ | $\hat{D}_{dam}$ |
| A | 12/230 | 5/230 | 2/195 | 1/155 | {5} | {10%} |
| B | 65/303 | 4/266 | 2/266 | 2/266 | {4,5,9} | {10%,10%,10%} |
| C | 10/213 | 4/155 | 2/193 | 3/193 | {9,20} | {10%,10%} |
| D | 6/155 | 5/155 | 3/155 | 2/155 | {28} | {20%} |
| E | 1/303 | 1/299 | 1/266 | 1/303 | {25,30} | {10%,10%} |
| F | 2/303 | 1/266 | 1/374 | 1/303 | {9,25} | {10%,10%} |
| G | 1/230 | 1/267 | 1/267 | 1/267 | {35,38} | {10%,10%} |
| H | 1/337 | 1/337 | 1/337 | 1/266 | {25,26} | {10%,10%} |

[a] The damage cases here are identical to the previous damage cases in Table 6.
[b] The first number is the rank of the actual damage case and the second is the total number of the examined hypotheses.
[c] c$\hat{L}_{dam}$ and $\hat{D}_{dam}$ are identified using all the four load patterns and $N_s = 20$.

### *3.3.2. Diagnoses of damage cases with modeling error and measurement noise*

In Table 8, the previous damage cases are re-diagnosed: (1) using all four load patterns; (2) considering both modeling error and measurement noise; and (3) increasing the number of data sets ($N_s$) from 1 to 20. To simulate the measurement noise, the analytical Ritz vectors generated from the baseline structure are perturbed with a 5% noise level using Eq. (31). Table 8 shows that: (1) the diagnoses provided by the proposed method improve as the number of data sets increases; and (2) if load patterns are selected carefully and a large number of data sets are available, the proposed method can identify the actual locations and amount of damage even in the presence of measurement noise and modeling error.

## 4. Conclusion and discussion

In this paper, load-dependent Ritz vectors are applied to a Bayesian probabilistic approach to detect the locations and amount of damage. Several damage scenarios using an eight-bay truss and a five-story frame structure illustrate the potential use of load-dependent Ritz vectors for damage detection. Sensitivity analyses show that the derived derivative of a load-dependent Ritz vector with respect to a substructure stiffness is a good approximation of the actual sensitivity, and the sensitivity analyses allow us to identify detectable substructures before actual diagnoses. The diagnosis results of the truss and frame structures show that: (1) load-dependent Ritz vectors are able to identify the actual damage locations for most damage cases when the estimated Ritz vectors are contaminated by 5% noise, only one set of Ritz vectors are estimated, and a small amount of stiffness deterioration (10% stiffness loss) is assumed; (2) by a careful selection of load patterns, substructures of interest can be made more observable using the Ritz vectors generated from the particular load patterns; (3) the proposed weighting scheme, which weights Ritz vectors according to their sensitivity to the assumed damage locations, improves the diagnosis results; and (4) if load patterns are selected carefully and a large number of data sets are available, the proposed method can identify most of the damage locations, even in the presence of modeling error and measurement noise.

While this paper has illustrated the potential applicability of load-dependent Ritz vectors to damage detection, many interesting research issues remain. First, even though a procedure to experimentally extract load-dependent Ritz vectors is proposed [2] and the effect of noise on the estimated load-dependent Ritz vectors is studied [20], real

testings should be conducted to validate the experimental procedure. Second, the physical issue of the actuator placement should be addressed to make the extraction of load-dependent Ritz vectors practical. In this paper, we assume that the amplitudes and phases among actuators can be fully controlled and the power requirement to generate the desired excitation forces is not addressed. Third, it is worth while to develop a systematic scheme to find load patterns, which yield better detection of damage in substructures of interest. While it is shown that a careful selection of load patterns can make the substructures of interest more observable, a systematic selection scheme for the load patterns has not been addressed.

## Acknowledgements

This research is partially sponsored by the National Science Foundation under Grant No. CMS952612. Valuable discussions with Professor Anne S. Kiremidjian and Mr Erik G. Straser at Stanford University are sincerely appreciated. The authors also wish to express their sincere thanks to Professor David C. Zimmerman of the University of Houston and Dr Timothy T. Cao of the NASA Johnson Space Center for helpful discussions on the extraction procedure of Ritz vectors and Dr. Scott W. Doebling of the Los Alamos National Laboratory for providing the experimental and analytical data of the eight-bay truss.

## References

[1] Cao TT, Zimmerman DC. Application of load-dependent Ritz vectors in structural damage detection. In: The Proceeding of the 15th International Modal Analysis Conference, Orlando, FL, 1997. p. 1319–24.

[2] Cao TT, Zimmerman DC. A procedure to extract Ritz vectors from dynamic testing data. In: The Proceedings of the 15th International Modal Analysis Conference. Orlando, FL, 1997. p. 1036–42.

[3] Doebling SW, Farrar CR, Prime MB, Shevitz DW. Damage identification and health monitoring of structural and mechanical systems from changes in their vibration characteristics: A literature reviews. Technical Report LA13070MS, Los Alamos National Laboratory, Los Alamos, NM, 1996.

[4] Doebling SW, Hemez FM, Barlow MS, Peterson LD, Farhat CR. Selection of experimental modal data sets for damage detection via model update. Technical Report AIAA931481CP, American Institute of Aeronautics and Astronautics, 1993.

[5] Ewins DJ. Modal Testing: theory and practice. New York: Wiley, 1995.

[6] Farrar CR, Cone KM. Vibration testing of the I-40 bridge before and after the introduction of damage. In: The Proceedings of the 13th International Modal Analysis Conference, Nashville, TENN, 1995. p. 203–9.

[7] Farrar CR, Doebling SW, Cornwell PJ, Straser EG. Variability of modal parameters measured on the Alamosa Canyon Bridge. In: The Proceedings of the 15th International Modal Analysis Conference, Orlando, FL, 1997. p. 257–63.

[8] Farrar CR, Jauregui D. Damage detection algorithms applied to experimental and numerical modal data from the 140 bridge. Technical Report LA13074MS, Los Alamos National Laboratory, Los Alamos, NM, 1996.

[9] Fukunaga K. Introduction to statistical pattern recognition. New York: Academic Press, 1990.

[10] Garcia GV, Stubbs N. Relative performance evaluation of pattern recognition models for nondestructive damage detection (NDD). In: The Proceedings of the 15th International Modal Analysis Conference, Orlando, FL, 1997. p. 1822–30.

[11] Kashangaki TA-L. Ground vibration tests of a high fidelity truss for verification of on orbit damage location techniques. Technical Report NASATM107626, National Aeronautics and Space Administration, 1992.

[12] Kashangaki TA-L, Smith SW, Lim TW. Underlying modal data issues for detecting damage in truss structures. Technical Report AIAA922264CP, American Institute of Aeronautics and Astronautics, 1992.

[13] Kim HM, Craig RR. Application of unsymmetric block Lanczos vectors in system identifications. International Journal of Analytical and Experimental Modal Analysis 1992;7:227–41.

[14] Leger P, Wilson EL, Clough RW. The use of load-dependent Ritz vectors for dynamic and earthquake analyses. Technical Report UC13/EERC86/04, Earthquake Engineering Research Center, University of California Berkeley, Berkeley, CA, 1986.

[15] Pandey AK, Biswas M, Samman MM. Damage detection from changes on curvature mode shapes. Journal of Sound and Vibration 1991;145:321–32.

[16] Ricles JM, Kosmatka JB. Damage detection in elastic structures using vibratory residual forces and weighted sensitivity. American Institute of Aeronautics and Astronautics 1992;30:2310–6.

[17] Sohn H, Law KH. Bayesian probabilistic approach for structure damage detection. Earthquake Engineering and Structural Dynamics 1997;26:1259–81.

[18] Stubbs N, Kim JT, Topole K, An efficient and robust algorithm for damage localization in offshore platforms. In: ASCE Tenth Structures Congress, San Antonio, TX, 1992. p. 543–6.

[19] Yao GC, Chang KC, Lee GC. Damage diagnosis of steel frames using vibrational signature analysis. Journal of Engineering Mechanics 1992;118:1949–61.

[20] Zimmerman DC, Cao TT. Effects of noise on measured Ritz vectors. In: The Proceedings of 1997 ASME Design Engineering Technical Conferences, Sacramento, CA, 1997.